

VERIFICATION OF MODELLING OF FLUID- STRUCTURE INTERACTION (FSI) PROBLEMS BASED ON EXPERIMENTAL RESEARCH OF BLUFF BODY OSCILLATIONS IN FLUIDS

O. Kotsur*, G. Scheglov**, P. Leyland***

* Ph. D student, Bauman Moscow State Technical University, visiting student EPFL,

** Professor, Bauman Moscow State Technical University

*** Interdisciplinary Aerodynamics Group, Ecole Polytechnique Fédérale de Lausanne, EPFL

Abstract

The comparison of the experimental and numerical results is presented for the free oscillation pendulum problem in a water tank. The results to be compared include pendulum dynamics information, in particular the evolution of the amplitude of oscillation, and velocity and vorticity fields that can be provided with the help of Particle Image Velocimetry (PIV) technology. The dynamics of the pendulum, which represent a classical Fluid-Structure Interaction (FSI) problem, is directly characterised by the system of vortices and coherent vortex structures, which are created in the process. The main aim of the paper is to compare these coherent structures, provided by the experiments and by those obtained using a chosen FSI numerical method.

1 Introduction

Bluff body dynamics are particularly challenging to reproduce both experimentally and computationally due to the extensive regions of unsteady separated flow and complex vortex shedding structures. Indeed, it is fundamental to understand the role of the different variables, and the problem is bilateral between the unsteady flow induced by a moving body (forced oscillations) and the flow induced oscillations as in vortex-induced vibrations, (VIV), [1].

In this paper, a forced oscillation is induced to a cylindrical pendulum geometry placed in a water tank. The pendulum movement induces a complex flow and vortex shedding within the

tank, that is monitored using a PIV system (LaVision),

The computational method used in this paper is based on a Finite Volume Method (FVM) with deformable meshes whose main benefit is their simple realisation on the basis of existing CFD codes that work on fixed meshes. However, it is not free from disadvantages imposed by the use of the computational mesh itself. Furthermore, large displacements of the immersed body can cause mesh degeneration and distortion, which results in compatibility and convergence problems. Although such techniques induce high computational cost and high disk memory requirements they remain the most widely used ones for FSI problems. A vortex method has also been developed. These techniques preserve the bilateral nature of the phenomena and remain close to the true induced forces. These results are presented in [2].

The more classical FVM computational set-up here is made using the open-source toolbox OpenFOAM.

The numerical and experimental results are discussed for the pendulum problem in a water tank, and conclusions are made on the effectiveness of the underlying mesh methods for an FSI problem.

2 Problem description

The problem of free pendulum oscillations in initially static viscous medium is a classical Fluid-Structure Interaction (FSI) problem. In conjunction with its relative intuitive simplicity it represents a sufficiently complex problem to study and to verify numerical methods of FSI.

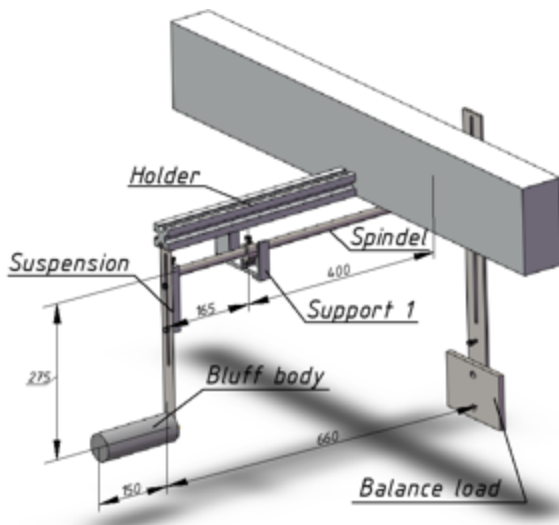


Fig. 1. 3D-model of the pendulum test rig

The experimental test rig is depicted in the Figure 1.

The simplicity of the pendulum test rig makes it possible to provide an experiment, in which both pendulum dynamics and valuable information about the coherent vortex structures can be studied. All these information can be obtained using Particle Image Velocimetry (PIV) technology [3], being one of the most effective means to study velocity and vorticity fields in flows of different nature.

The 3D-model of the test rig is illustrated above in the Figure 1. In this study a cylinder ($\varnothing 50\text{mm} \times 150\text{mm}$) plays role of a ‘bluff’ body that oscillates in an aquarium with water (see Figure 2); a standard balance load is used to change the inertia of the system.

To avoid unnecessary friction in supports, special ‘knife’ joints were used.

The mechanical and geometrical parameters of the pendulum system are given in Table 1.

A typical experimental test supposes an initial inclination of the pendulum at angle of 30° and free oscillations for a period of 30 seconds.

The same mechanical parameters, initial inclination and duration are chosen for numerical simulation.

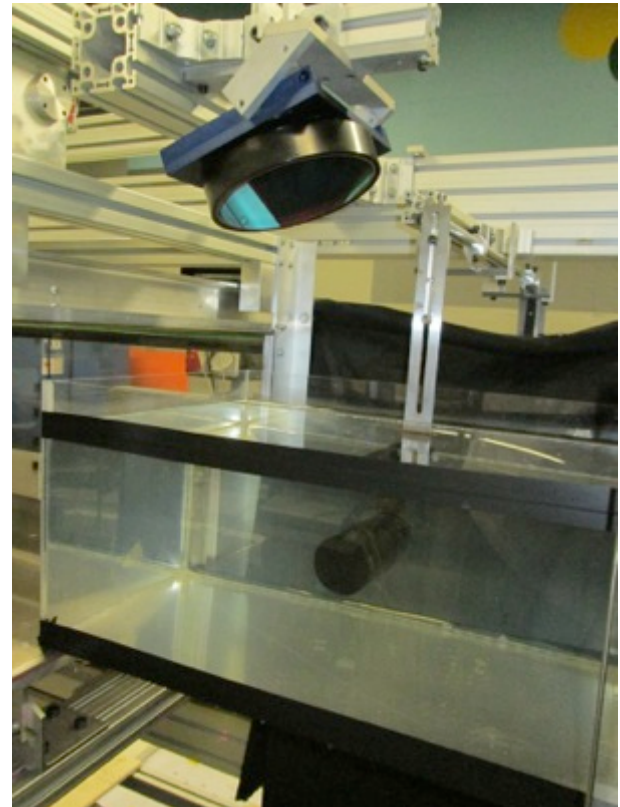


Fig. 2. Aquarium installation; note the controlling mirror for shadow effects.

Table 1. Pendulum parameters

Total mass M , g :	3511
Moment of inertia with respect to axis of rotation J , $g \cdot \text{mm}^2$:	366.2
Buoyancy force, F_a , N	3.155
Distance to the center of mass from axis of rotation l_c , mm :	229
Distance to the center of bluff body from axis of rotation l_p , mm :	0.279
Distance to the center of buoyancy force application from axis of rotation l_a , mm :	0.274
Proper frequency ν , Hz :	0.74

3 PIV set-up description

To study the structure of the vortex systems, their origin, emission and evolution, requires the knowledge of the velocity field of the induced flow around the bluff body. For these purposes PIV stays one of the most promising non-intrusive measurement technologies. The idea of this method is to add some ‘seeding’ into the flow in the form of small particles (around $10\mu\text{m}$ in diameter),

which follow the streamlines. They are illuminated two times within a short delay of time by a laser sheet. These two illuminations are photographed, and two acquired images are then processed using statistical cross-correlation methods to find the particles displacement between the first and the second illumination. In this way, the complete velocity field is provided within the region of interest.

The pulsed laser is placed below the aquarium, which has transparent bottom to let laser beam pass through. If the bluff body is illuminated from below, a shadow is created above with the water surface reflections. Therefore, a mirror is installed above the pendulum (fig. 2), to illuminate the pendulum from the top to avoid this shadow.

The experiments have been conducted using LaVision PIV system, which included two-pulsed Nd:YAG laser with the maximum frequency of 15 Hz, one or two double shutter cameras Imager SX 4M, a synchronization system and the DaVis 8.2 software, used both to acquire and to process PIV-images. In these experiments a single camera was used.

4 Numerical methods: The deformable mesh approach, implemented in OpenFOAM

Actually, a wide range of different numerical approaches is used to simulate FSI problems; see for example [4],[5],[6]. Among them one can mainly emphasise FVM with deformable meshes[4], moving ‘CHIMERA’ meshes, immersed boundary method (IBM) [7], vortex element methods and others. In this paper commonly used FVM-based method with deformable mesh is used [4].

The Partitioned approach [6] for FSI problems consists in the decomposition of the solution process into the fluid simulation block and the solid simulation block, which evolve along their own time iterative procedures and are updated together at the same equivalent physical time step, as the mechanism of their coupling.

The deformed time dependant mesh approach requires introduction of a third block in this sequence, which treats mesh deformation that “follows” the moving body. [8]- It should

be noted that this is automatically satisfied if the unsteady fluid equation system takes into account the mesh movement using an ALE approach into its numerical fluxes, and that the energy and geometric conservation is enforced. The algorithm can be represented as a sequence on three blocks being calculated iteratively:

1. Fluid domain block

- Solution of Navier-Stokes equations using a FVM;
- Calculation of the forces, distributed on the surface of a body.

2. Solid domain block

- Solution of the elasticity equations;
- Calculation of the displacement field of the immersed body’s surface.

3. Mesh deformation block

- Solution of the mesh deformation equation;
- Reconstruction of the mesh in correspondence with new body position.

In the present application, the mesh deformation equation to be solved is a Laplace equation for the new position of the mesh nodes after deformation.

Mesh deformation imposes major difficulties in itself for FVM. The main problem consists in the over distortion of the individual control finite volumes, which results in loss of quality and precision of gradient terms when the body moves with a large amplitude. Not only this results in loss of convergence rate, but also can render inconsistent the FVM. To avoid such mesh distortion a simple remedy is to enlarge the calculation domain to be much larger than the dimensions of aquarium.

This algorithm has been implemented on the basis of the C++ code OpenFOAM [9]. This code has modular structure, which simplifies coupling of fluid and solid solvers, as well as the mesh deformation block.

For the unsteady fluid system, the solver is based on the PIMPLE (merged PISO-SIMPLE [9]) algorithm, and for the mesh deformation part, the Laplace equation is solved as in [4, 8, 6]. Both parts are taken from the *pimpleDyMFoam* solver. The solid dynamics

part is written explicitly as a separate block and embedded into the solution scheme as explained before.

For the current pendulum problem, depicted schematically in Figure 3, the solid domain block is represented by a simple linear differential equation of the pendulum as given by Eq.(1), whose solution is well known Eq.(2):

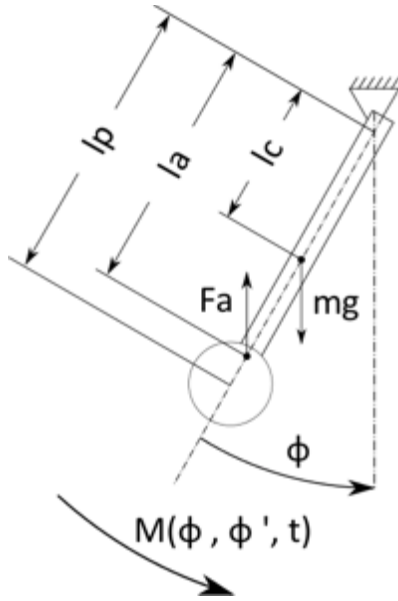


Fig. 3. Pendulum principal scheme

$$\ddot{\varphi}(t) + \omega^2 \varphi(t) = M(t_0) \quad (1)$$

$$\varphi(t) = \left(\varphi_0 - \frac{M(t_0)}{\omega^2} \right) \cos(\omega t) + \frac{\dot{\varphi}_0}{\omega} \sin(\omega t) + \frac{M(t_0)}{\omega} \quad (2)$$

where $M(t_0)$ stands for the moment of the force loading the pendulum, divided by its moment of inertia J , and taken at a time t_0 ; ω is the natural frequency; φ_0 and $\dot{\varphi}_0$ are the initial inclination and angular velocity respectively.

The natural frequency is calculated using the mechanical and geometrical pendulum parameters listed in the table 1 and depicted in the Figure 3, following the formula:

$$\omega = \sqrt{\frac{Mgl_c - F_a l_a}{J}} \quad (3)$$

This is then implemented under the assumption of linearity of the sine term, i.e. $\sin \varphi \approx \varphi$, which assumes small inclination angles, and results in the error of 2% for the initial inclination angle of 30° used in the simulation.

For every time step the fluid solver provides the forces, distributed over the surface of the bluff body, giving the initial condition $M(t_0)$ for equation (2), which in its turn calculates the angular displacement of the pendulum within a time step Δt . These data enter into the mesh deformation part to update it accordingly

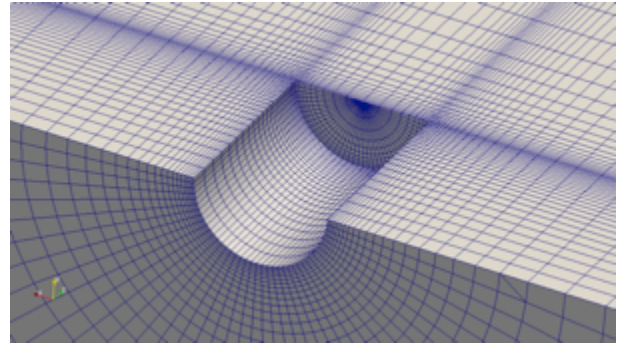


Fig. 4. Detail of part of the computational mesh at time t_0

The general assumptions and the simulation parameters that are taken here are:

- A simple linear dynamic model of the pendulum;
- The suspension bar is not modelled;
- The effect of the free water surface and proximity of aquarium walls are not taken into account;
- Two options are considered for Turbulence modelling:
 - a. LES – using a one equation model;
 - b. Laminar flow;
- The unstructured mesh is created with the *blockMesh* utility of OpenFOAM (see a detail in Figure 4);
- Computational domain dimensions in mm: $2400 \times 1600 \times 900$;
- Number and type of cells: 338000 cells that are mainly hexahedra;
- Average computation cost: 33 hours on 16 cores.

4. Principal results

In this section some principal results of the numerical simulations; the PIV experiments are also given as a comparison.

4.1 Pendulum dynamics

The pendulum free oscillation problem is a non-stationary problem, which acts over a wide range of Reynolds numbers. For every period the pendulum passes two main specific phases: the phase of the maximum linear velocity (A) when it passes its equilibrium position (Re is maximal); and a stop-phase (B) when the pendulum reaches its maximal amplitude (Re is minimal). The effective Reynolds number evolution in time is presented in the Figure 5. Here the number of Reynolds is calculated using cylinder diameter as a characteristic length and the maximal velocity attained by a lowest point of the cylinder during the period, which was considered as the characteristic velocity (fig.5). Each point here corresponds to the moment when pendulum passes the point of equilibrium.

For the pendulum-fluid model two kinds of simulations were made: one using a LES turbulence approximation and one using a laminar model. On the figures 6 and 7 an integral dynamic process of amplitude damping is shown; fig. 6 corresponds to the LES model and fig. 7 to the laminar model.

As it can be noticed, the two models work differently in different ranges of numbers of Reynolds. At the beginning the flow around the pendulum can be considered as highly turbulent, or even chaotic.

These results agree with the experiment quite well during the first two periods of oscillation. However, subsequently, the LES model imposes an excessive viscosity in the flow, which results in increased pendulum damping. Whereas with the laminar model we observe that the opposite phenomena occur. The amplitude evolution curves diverge in the beginning phase (1st-4th periods), where neglecting the effect of turbulence results in a lack of drag. However, when the amplitude angle is less than 8°-9°, then this model works better than taking an LES one.

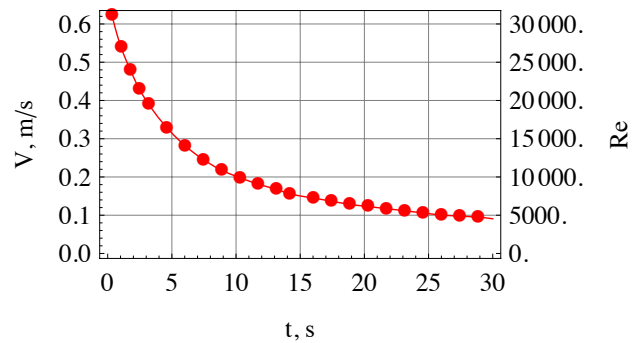


Fig. 5. Maximal linear velocity and Reynolds number evolution

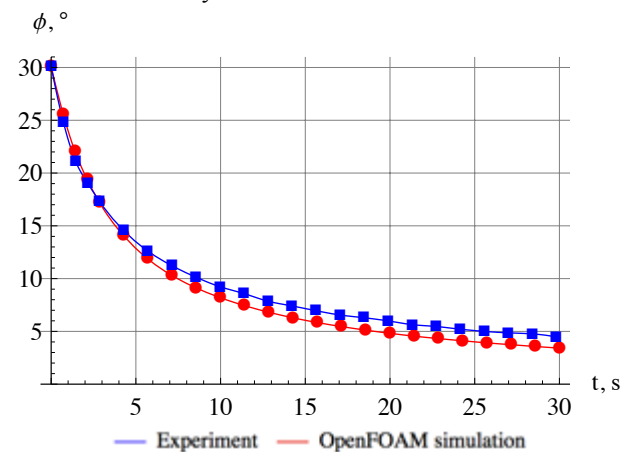


Fig. 6. Pendulum amplitude evolution using a LES-model

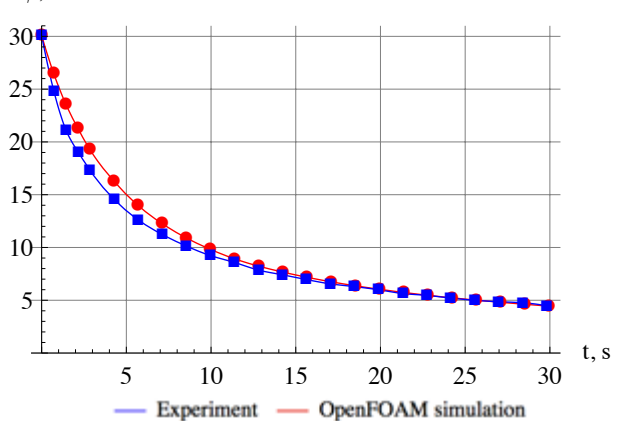


Fig. 7. Pendulum amplitude evolution using a laminar model

4.2 Regular flow structures

First, a system of big coherent vortex structures is generated through the pendulum oscillating motion. During the creation process, the vortexes accumulate a considerable amount of energy, which is transferred directly from the pendulum. Then, after separation, these vortexes act like independent energy and flow sources which interact, until they dissipate, with the

bluff body. Hence, the dynamics of the pendulum are mostly determined by these coherent structures, generated by the pendulum itself rather than the viscous friction on the surface. Therefore, the study of these structures, as well as their correct simulation is essential. In order to visualize the results, two section planes were chosen (fig. 8). The first one corresponds to the midsection of the cylinder ($z=0$ mm), where the velocity field exhibits "in-plane" characteristics, and a second one ($z=58$ mm), which shows the 3D-boundary effects occurring at the end of the cylinder.

Further, as the pendulum oscillation is a periodic process, one can divide a period into phases which correspond to specific angular positions of the pendulum. As a result, one can emphasize two specific positions of the pendulum which are of particular interest (fig. 9). The first one, denoted as "*Phase A*", corresponds to the equilibrium point where the maximum velocity is reached, and the second one, denoted as "*Phase B*", corresponding to the maximum angular position of the pendulum. In this study the "*Phase A*", corresponds to the first quarter of the first period (i.e. $t=0.36s$), and "*Phase B*" corresponds to the end of the first period of oscillation (i.e. $t=1.41s$).

The results of the numerical simulations and the experimental studies in both section planes are presented in figures 10-17 for Phase A, and in figures 18-25 for Phase B. The visualisation of the flow structure is obtained using a velocity magnitude colour-map and the local mean of the velocity vector field. Furthermore, one can use the streamlines to approximate the position of the vortexes cores centre, which can be used as a criterion to compare both experimental and numerical studies.

Figures 22 and 23 show vortex positions on a more wide area around the cylinder than shown on figures 20 and 21.

One should notice that, for zones close to the cylinder tip, the "out of plane" component is predominant, which is one of the limits of the 2D-PIV encountered in this study. The resulting streamlines for *Phase A*, presented in fig. 16-17,

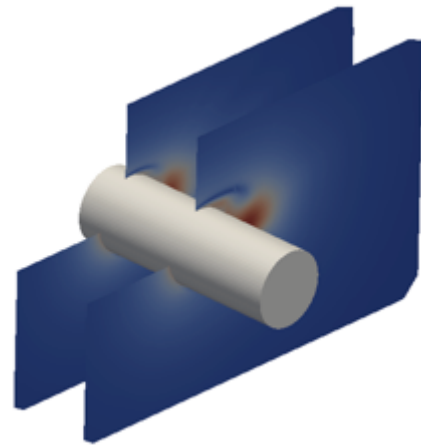


Fig. 8. Section planes for visualization of the results

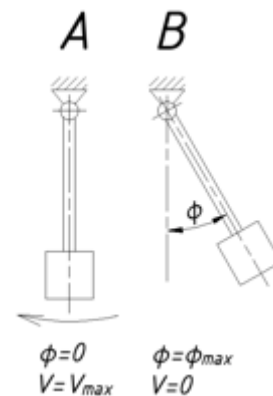


Fig. 9. Phase A and phase B where the flow was studied

are based on that in-plane velocity component and one can clearly see the presence of an in-plane vortex tip in the wake of the cylinder (fig. 17). Regarding *Phase B*, the streamlines are not clearly visible as the flow following the pendulum searches a way to "continue" its movement while the pendulum has already stopped. This results in a high "out of phase" velocity component, and in this particular case the use of in-plane streamlines to visualize the flow is meaningless.

Streamlines, based on the in-plane velocity components, are shown (fig. 16-17). On the figure 17 an in-plane vortex tip can be clearly seen in the wake of the cylinder, which reaches with its maximal speed.

However, the streamlines are not shown for the *phase B*, because the flow, following the pendulum, searches the ways to continue its movement, while the pendulum has already stopped. This results in a very high domination of out-of-plane velocity component. In this case the use of in-plane streamlines to visualize the flow is out of sense.

VERIFICATION OF MODELLING OF FLUID-STRUCTURE INTERACTION (FSI) PROBLEMS
 BASED ON EXPERIMENTAL RESEARCH OF BLUFF BODY OSCILLATIONS IN FLUIDS

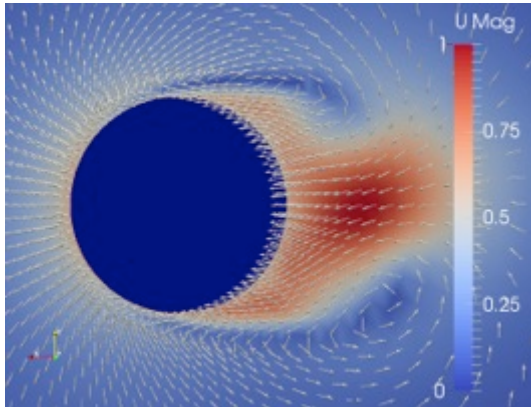


Fig. 10. Velocity field. Phase A ($t = 0.36 \text{ s}, z = 0 \text{ mm}$)

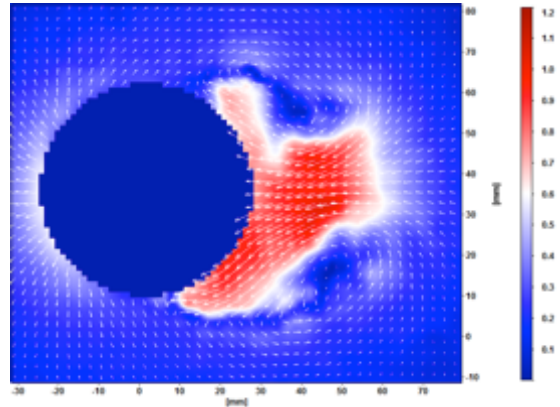


Fig. 11. *PIV experiment*. Velocity field. Phase A ($t = 0.36 \text{ s}, z = 0 \text{ mm}$)

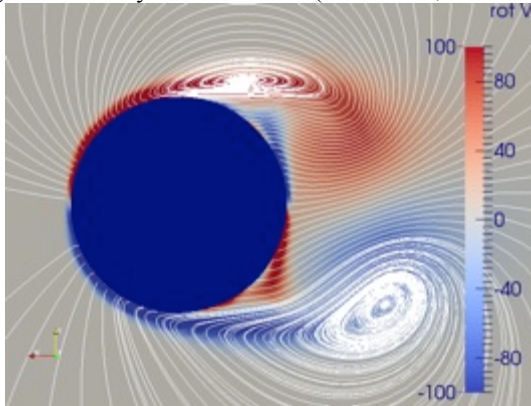


Fig. 12. Streamlines and vorticity field. Phase A ($t = 0.36 \text{ s}, z = 0 \text{ mm}$)

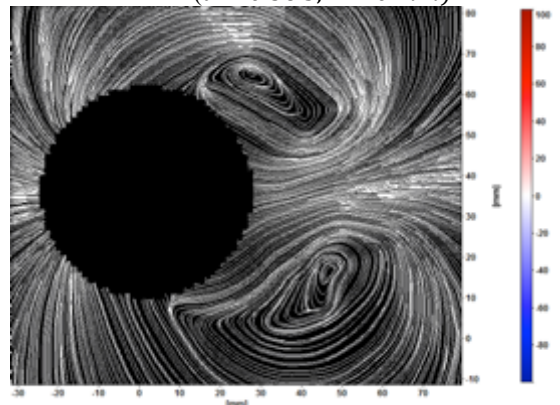


Fig. 13. *PIV experiment*. Streamlines. Phase A ($t = 0.36 \text{ s}, z = 0 \text{ mm}$)

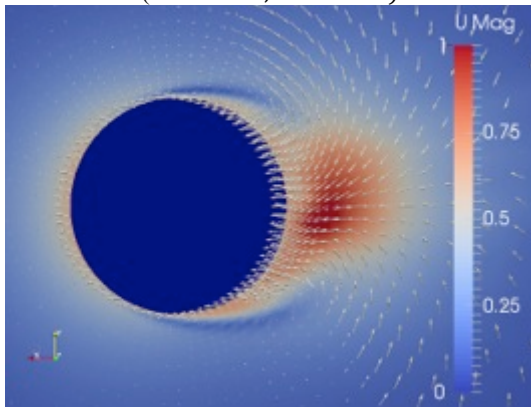


Fig. 14. Velocity field. Phase A ($t = 0.36 \text{ s}, z = 58 \text{ mm}$)

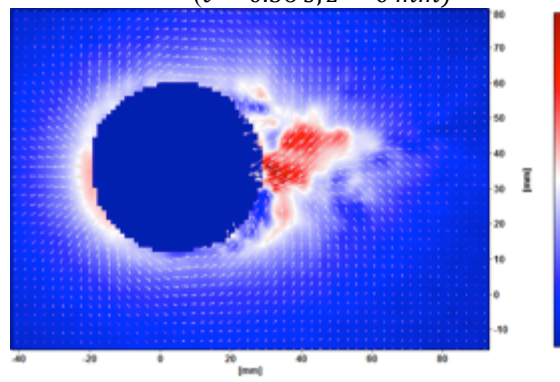


Fig. 15. *PIV experiment*. Velocity field. Phase A ($t = 0.36 \text{ s}, z = 58 \text{ mm}$)

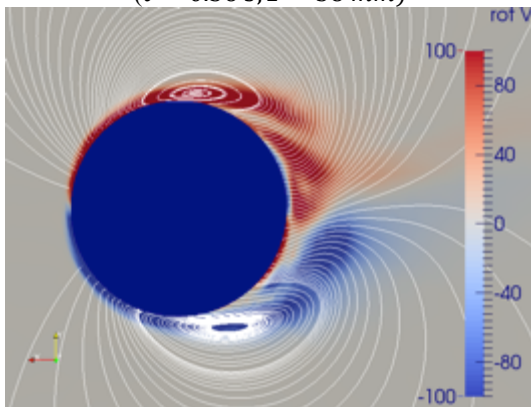


Fig. 16. Streamlines and vorticity field. Phase A ($t = 0.36 \text{ s}, z = 58 \text{ mm}$)

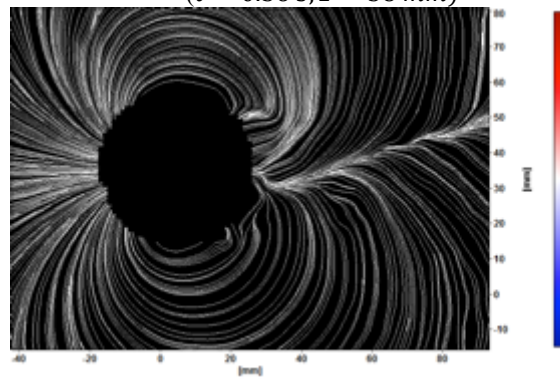


Fig. 17. *PIV experiment*. Streamlines and vorticity field. Phase A ($t = 0.36 \text{ s}, z = 58 \text{ mm}$)

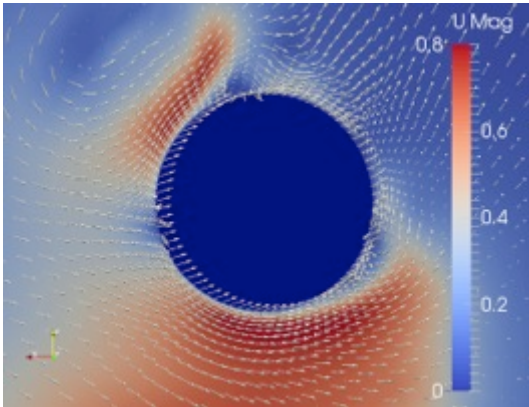


Fig. 18. Velocity field. Phase B ($t = 1,41 \text{ s}, z = 0 \text{ mm}$)

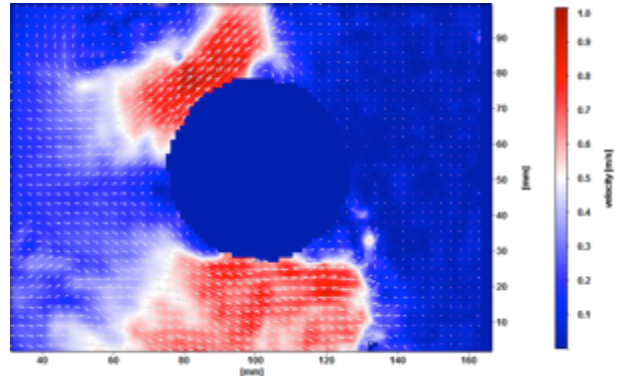


Fig. 19. *PIV experiment*. Velocity field. Phase B ($t = 1,41 \text{ s}, z = 0 \text{ mm}$)

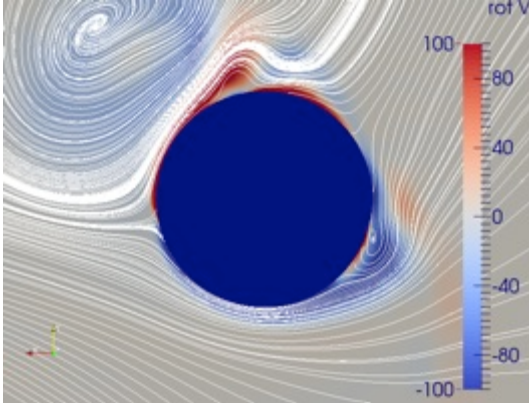


Fig. 20. Streamlines and vorticity field. Phase B ($t = 1,41 \text{ s}, z = 0 \text{ mm}$)

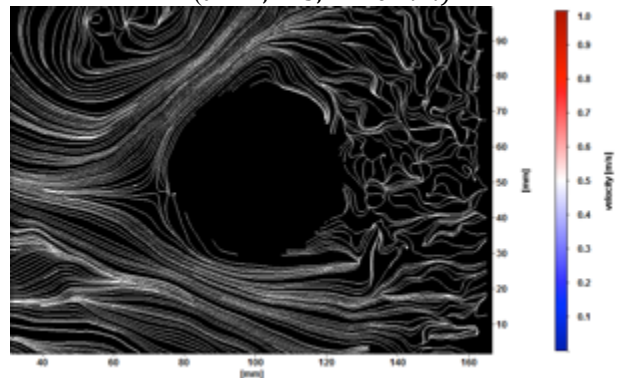


Fig. 21. *PIV experiment*. Streamlines and vorticity field. Phase B ($t = 1,41 \text{ s}, z = 0 \text{ mm}$)

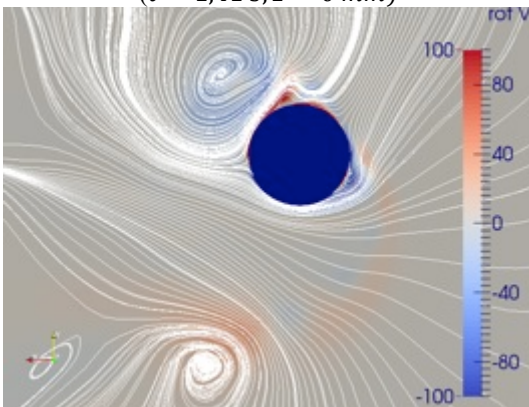


Fig. 22. Two vortices near the cylinder. Phase B ($t = 1,41 \text{ s}, z = 0 \text{ mm}$)

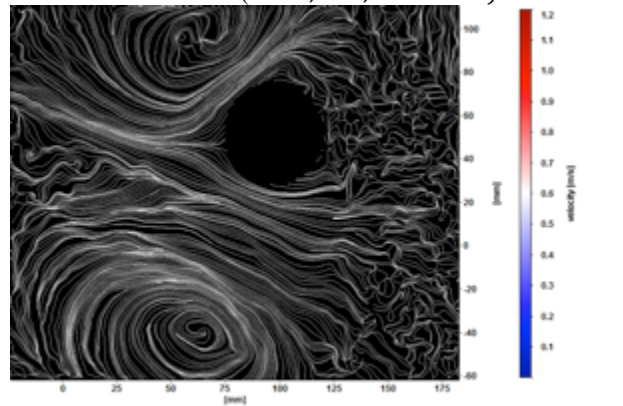


Fig. 23. *PIV experiment*. Two vortices near the cylinder. Phase B ($t = 1,41 \text{ s}, z = 0 \text{ mm}$)

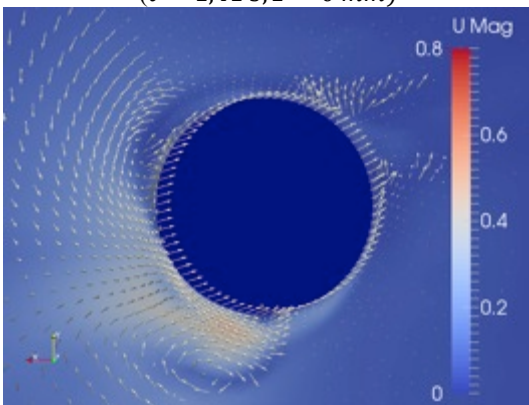


Fig. 24. Velocity field. Phase B ($t = 1,41 \text{ s}, z = 58 \text{ mm}$)

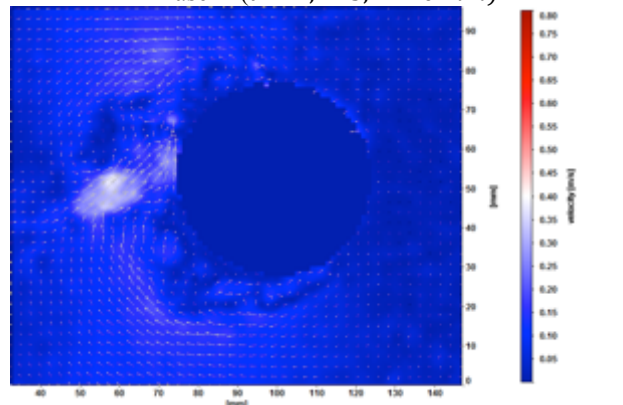


Fig. 25. *PIV experiment*. Velocity field. Phase B ($t = 1,41 \text{ s}, z = 58 \text{ mm}$)

5 Numerical aspects of the simulation and analysis of the results

As it was mentioned before, the dynamics of the pendulum simulation depend significantly on correctness of the vortex system description, i.e. vortex intensity and lifetime. When adopting a moving FVM method, this requires a very fine mesh of good quality, refined everywhere where vortices exist. Otherwise, only the most substantial vortices are captured, whereas the small ones either are not 'seen' by the solver, or are dissipated rapidly by numerical effects.

However, as practice shows for such pendulum FSI problem, the use of well-refined meshes of more than 2 million cells meets two principal problems. Both of them are connected to the limitations of FSI problems when solved with FVM with deformable meshes.

Firstly, when the mesh is too fine, use of an explicit iterative procedure leads to very low stability criteria and numerical instabilities arise. The very small cells have a relative distortion that can be larger than bigger cells during the deformation process. This is particularly the case when boundary layers are present where the flow gradients are not optimally approached on such distorted cells. This results in globally poor mesh quality when the pendulum reaches its maximal amplitude, and which results, in its turn, either very slow convergence to equilibrium, or no convergence at all.

The second main problem consists in very high computational costs. When the solution scheme contains the mesh deformation block, it takes much more time to deform the mesh as number of cell grows.

The above simulations were made on the 3D-mesh of 338000 cells, which is insufficiently refined enough to capture very well the thin vortical structures. However, the equivalent of 30 seconds of real time took already over 32 hours of computer time on 16 cores ($\approx 1,1$ hour / 1 sec of simulation). For comparison, the same simulation was made for a mesh of 1019760 cells, taking 205 hours on 32 cores to model 30 seconds of the pendulum oscillations ($\approx 6,8$ hours / 1 sec of simulation).

These limitations for using the so-called 3-field approach with the mesh field method for large deformations and considerable body displacement are classical. Nevertheless, the 338000 cells mesh show from the figures 6-7 the good agreement of the amplitude damping between OpenFOAM and the experiments. This is partially due to the vortex dominance of such flows, as the vortical core positions correspond to total pressure "holes", which can be well estimated by inviscid approximations, hence the influence of insufficiently describing the boundary layer characteristics is not evident.

As it was assumed before, using a turbulent model (LES) works well at the beginning phase of oscillation. In this phase the difference from the experiments stays up to 6% for the first 5 periods, going up to 25% for the remainder of the simulation. In fact, for the first two periods the real pendulum exposes more intensive drag, than its numerical model for both LES and the laminar models, which can be partially explained by presence of the suspension bar, on which the cylinder is fixed. This creates a small additional drag, which is significant for the first periods of an intensive transient process.

Comparison with the PIV-results shows good agreement. For the middle cylinder section the velocity vector fields have similar configurations (fig. 18, 19). The streamlines show quite good coincidence of the vortex cores position between the experiment and the simulation (fig. 20, 21). The real flow turns out to be a little less regular, and more chaotic, than the simulated one. Small vortices, small zones of non-regular, turbulent/chaotic flow can be distinguished, whereas the simulation captures only the large-scale structures. Small-scale objects are cannot be resolved well on the actual mesh, which is rather coarse as mentioned above.

The same conclusions can be noticed for the side section (fig. 22-25). For the phase B a small difference can be seen between the experiment and the simulation for the side section ($z = 58$ mm). This can be explained by looking at the out-of-plane velocity, whose in-plane components have small values, which increase the error of vector calculation in the PIV postprocessing phase.

6 Conclusions

In this work, the problem of free pendulum oscillations was simulated using a FVM with deformable meshes. This approach was realised using the OpenFOAM open-source tool. The existing *pimpleDyMFoam* solver was adapted for the pendulum problem with the addition of pendulum dynamics equation.

This approach has shown good agreement with the experiment, taking the amplitude evolution as a main criterion. Some differences are distinguished between laminar and turbulent modelling solutions, which can be explained by a wide range of Reynolds number of the process with turbulence effects dominating at the beginning, and the discrepancies between the mesh resolution and the viscous modelling in general.

Several important drawbacks of the 3-field mesh approach were discovered. Among them there are:

- Necessity to calculate mesh motion every time step;
- High possibility of mesh degeneration during its motion when pendulum reaches its amplitude; this is the main reason that limits the use of high-resolution meshes;
- Convergence problems on distorted mesh;
- Very high computational costs and memory requirement even on coarse meshes, which also limits the use of such an approach on real engineering large-scale problems.

Taking in account its benefits and drawbacks, the so called “mesh” method can turn to be efficient for small deformation problems of aeroelasticity, FSI problems where displacements of body’s surface are small, and when the computational domain is not too big. The bodies can be taken to be either rigid, or elastic, with the boundary surface moving arbitrarily.

7 Future research

The Vortex Element Method (VEM), which does not require a computational grid, seems to be more appropriate for this particular type of problem, where the correct description of vorticity and vortexes in the flow is of the most

importance. Future research consists in verification of VEM with the same experimental results. Comparison with FVM approach and analysis of effectiveness of both mesh and mesh-free approaches is planned.

References

- [1] C.H.K. Williamson and R. Govardhan; *Vortical Induced Vibrations, Annu. Rev. Fluid Mech.* 36:413–55. 2004
- [2] O. Kotsur et al. The Vortex Element Method for Bluff Body induced Vortex Systems. *In Preparation.*
- [3] Raffel M, Willert C, Wereley S, and Kompenhans J. *Particle Image Velocimetry. A Practical Guide.* Springer, 2007.
- [4] Jasak H and Tukovic Z. Automatic mesh motion for the unstructured finite volume method. *Transactions of FAMENA*, 30(2):1–20, 2006.
- [5] H. Blackburn; *Computational Bluff Body Fluid Dynamics and Aeroelasticity; Coupling of Fluids, Solids and Waves Problems in Aeronautics*, Springer 2002.
- [6] P. Leyland and V. Carstens: Strongly Coupled Fluid Structure Interaction Methods_ Flutter investigations in Compressor Cascades. *Fluid-Structure Interaction* ed. Hermes, 2000.
- [7] Hou G, Wang J and Layton A. Numerical Methods for Fluid-Structure Interaction — A Review. *Commun. Comput. Phys.*, Vol. 12, No.2, pp. 337-377, 2012.
- [8] C. Farhat, P. Geuzaine and G. Brown, *Application of a Three-Field Nonlinear Fluid-Structure Formulation to the Prediction of the Aeroelastic Parameters of an F-16 Fighter*, *Computers and Fluids*, Vol. 32, pp. 3-29 (2003)
- [9] Jasak H. *Error analysis and estimation for the finite volume method with applications to fluid flows.* PhD thesis, Imperial College of Science, Technology, and Medicine, 1996.

Copyright Statement

The authors confirm that they, and/or their company or organization, hold copyright on all of the original material included in this paper. The authors also confirm that they have obtained permission, from the copyright holder of any third party material included in this paper, to publish it as part of their paper. The authors confirm that they give permission, or have obtained permission from the copyright holder of this paper, for the publication and distribution of this paper as part of the ICAS 2014 proceedings or as individual off-prints from the proceedings.